Highly-parallel microfluidics-based force spectroscopy on single cytoskeletal motors

Marta Urbanska[1,†], Annemarie Lüdecke[1,§], Wim J. Walter[1,2], Antoine M. van Oijen[3,4], Karl E. Duderstadt[3,5,6,], Stefan Diez[1,7,8,*]*

[1]B CUBE - Center for Molecular Bioengineering, Technische Universität Dresden, 01069 Dresden, Germany

[2]Biozentrum Klein Flottbek, Universität Hamburg, 22609 Hamburg, Germany

[3]Zernike Institute for Advanced Materials, University of Groningen, NL-9700 AE, Groningen, Netherlands

[4]Centre for Medical and Molecular Bioscience, Illawarra Health and Medical Research Institute and University of Wollongong, Wollongong, 2522 New South Wales, Australia

[5]Structure and Dynamics of Molecular Machines, Max Planck Institute of Biochemistry, 82152 Martinsried, Germany

[6]Physics Department, Technische Universität München, 85748 Garching, Germany

[7]Cluster of Excellence Physics of Life, Technische Universität Dresden, 01062 Dresden, Germany

[8]Max Planck Institute of Molecular Cell Biology and Genetics, 01307 Dresden, Germany

[†]present address: Max Planck Institute for the Science of Light & Max-Planck-Zentrum für Physik und Medizin, 91058 Erlangen, Germany

[§]present address: NanoTemper Technologies GmbH, Flößergasse 4, 81369 München, Germany

*correspondence and requests for materials should be addressed to K.E.D. (email: duderstadt@biochem.mpg.de) and S.D. (email: stefan.diez@tu-dresden.de).

Abstract

Cytoskeletal motors transform chemical energy into mechanical work to drive essential cellular functions. Optical trapping experiments have provided crucial insights into the operation of these molecular machines under load. However, the throughput of such force spectroscopy experiments is typically limited to one measurement at a time. Here, we describe an alternative, highly-parallel, microfluidics-based method that allows for rapid collection of force-dependent motility parameters of cytoskeletal motors. We applied tunable hydrodynamic forces to stepping kinesin-1 motors via DNA-tethered beads and utilized a large field-of-view to simultaneously track the velocities, run lengths and interaction times of hundreds of individual kinesin-1 molecules under varying resisting and assisting loads. Importantly, the 16-μm long DNA tethers between the motors and the beads significantly reduced the vertical component of the applied force pulling the motors away from the microtubule. Our approach is readily applicable to other molecular systems and constitutes a new methodology for parallelized single-molecule force studies on cytoskeletal motors.

Keywords

single-molecule force spectroscopy, molecular motors, cytoskeletal motors, kinesin, microtubules

The application and detection of forces using single-molecule manipulation methods has provided major advances in our understanding of the operating principles of mechanoenzymes[1–4]. Optical and magnetic tweezers as well as atomic force microscopy are now being routinely used to study protein folding pathways, receptor-ligand interactions, DNA mechanics and the activity of molecular motors. While all of these experimental approaches offer excellent spatiotemporal resolution and force accuracy—with different force spectra and displacement ranges covered—none of them provides high experimental throughput as conventionally only one molecule is studied at a time. This limitation constitutes one of the major bottlenecks in current single-molecule force measurements[4,5], where the derivation of statistically significant results from stochastic single-molecule footprints is desired in reasonable time frames. Consequently, continuous efforts are being made to surpass this limitation in the field of optical[6–8] and magnetic trapping[9–11] as well as in atomic force microscopy—regarding both instrumental automation[12] and sample preparation[13]. Alongside, a number of novel solutions for multiplexed force manipulation, such as centrifuge force microscopy[14,15] and acoustic force spectroscopy[16], are being introduced. So far, the use of these novel methods has been demonstrated for the studies of DNA mechanics, DNA-protein binding and protein-protein binding but not for cytoskeletal motor proteins. While their use to study DNA motors is conceivable, they may require modifications to become applicable for studies on cytoskeletal motors because of the vertical character of the applied force.

One so far largely unexploited way to apply calibrated forces onto individual molecules is hydrodynamic flow. In a microfluidic environment, laminar flow can be used to exert Stokes drag on micrometer-sized beads that act as force handles when linked to surface-attached biomolecular mechanosystems. The magnitude of the drag force is determined by the diameter of the beads and the velocity of the flow. The latter can be kept constant over large regions in a microfluidic chamber. The response of the molecular system under investigation can then be deduced by tracking the positions of multiple beads simultaneously using an optical

microscope. Hence, the number of constant-force experiments performed at a time is in principle limited only by the size of the imaged area and the surface density of the bead-coupled mechanosystems. Low-throughput experiments using hydrodynamic flow have so far been performed to study single-molecule forces in protein unfolding[17], to measure rupture forces of streptavidin-biotin bonds[18], to investigate the confining potential felt by individual membrane-embedded receptors[19] and, in the context of cytoskeletal motors, to measure the adhesion forces of beads covered with multiple kinesin-1 motors to microtubules[20]. Moreover, high-throughput experiments using hydrodynamic flow have been performed to study DNA mechanics and DNA-protein interactions. In particular, highly-parallel measurements to monitor the enzymatic activity of DNA exonucleases[21], DNA and RNA polymerases[22–25], or topoisomerases[26] have been demonstrated on flow-stretched DNA, with force control down to 0.1 pN.

Here, we demonstrate the application of hydrodynamic forces to investigate the translocation of cytoskeletal motors under load in a highly parallel manner. In particular, we use paramagnetic beads attached to individual kinesin-1 motors via 16-μm long DNA linkers as force handles and utilized a large field-of-view microscope to characterize the velocities, run lengths and interaction times of hundreds of motors stepping under a series of in situ calibrated force conditions. Leveraging the large spatially homogenous force field generated by hydrodynamic flow and the use of a specialized telecentric lens capturing a field-of-view of several millimeters in size, we were able to optically track hundreds of individual molecules in a single experiment, amounting to a total of 2500 events in eight experiments. Consistent with previous low-throughput measurements with optical tweezers, our data shows that the velocity of kinesin-1 motors gradually decreased under increasing load by up to 60% for resisting loads of about 3 pN. For assisting loads of the same magnitude, the velocity decreased by up to 32%. Due to the molecular geometry of our assay, we were able to directly measure the motility parameters of kinesin-1 in the absence of significant vertical forces (i.e. away from the microtubule surface), which had previously been only accessible by theoretical calculations.

Our high-throughput method does not require expensive equipment and can be easily adapted to other biomolecular mechanosystems.

Results and Discussion

Molecular assembly of the mechanosystems. To assemble the molecular system for tracking of individual kinesin-1 motors stepping along microtubules under load, we sequentially attached specially designed molecular components to the surface of a flow cell by flowing them through the flow cell using a syringe pump (Figure 1a and Methods). First, GMPCPP-stabilized microtubules were immobilized on the surface via anti-β-tubulin antibodies. Next, truncated, SNAP-tagged kinesin-1 motors were covalently coupled to 16.2-μm-long double-stranded DNA (dsDNA) linkers based on lambda phage DNA (λ-DNA) with functionalized ends. The kinesin-DNA complexes were then introduced to the flow cell and attached to the microtubules under flow in the presence of 100 μM AMPPNP. Finally, 1-μm sized superparamagnetic beads coated with anti-digoxigenin antibodies were flowed in and attached to the free ends of the DNA linkers. The AMPPNP kept the kinesin-1 motors at fixed positions on the microtubules until the beginning of the measurement which was initiated by the addition of 10 mM ATP (Supplementary Figure 1). Evaluation of the extreme positions of the beads during flow reversal showed that the length of most tethers corresponds to the full length single λ-DNA (Supplementary Figure 2), indicating prevalence of full-length molecules with single attachment sites.

Microfluidics-based force assay. The heart of the experimental setup constituted a custom-made inverted microscope (Figure 1b). A syringe pump, operated in withdrawal mode, was used to apply a hydrodynamic flow throughout the experiment. An air spring was introduced between the flow cell outlet and the pump in order to damp any flow irregularities. To minimize interactions of the tethered beads with the surface, a magnet installed on the top of the flow cell provided a miniscule force of approximately 0.1 pN to lift the paramagnetic beads up. To observe the bead positions, the flow cell was illuminated from the side with high-intensity white

light from a fiber illuminator. The light scattered by the beads was collected through a telecentric lens and projected onto a CCD camera. Due to the large scattering cross-section of the beads it was possible to implement a low-magnification objective to maximize the field-of-view without substantial loss in accuracy when determining the bead positions. The high quality of the telecentric lens, together with the 29 Megapixel camera sensor, provided for distance-accurate imaging of an 18 mm^2 large region. Within one field-of-view it was possible to image up to 30,000 beads (Figure 1c) and each of them could be tracked with a precision of 32 nm (see Methods).

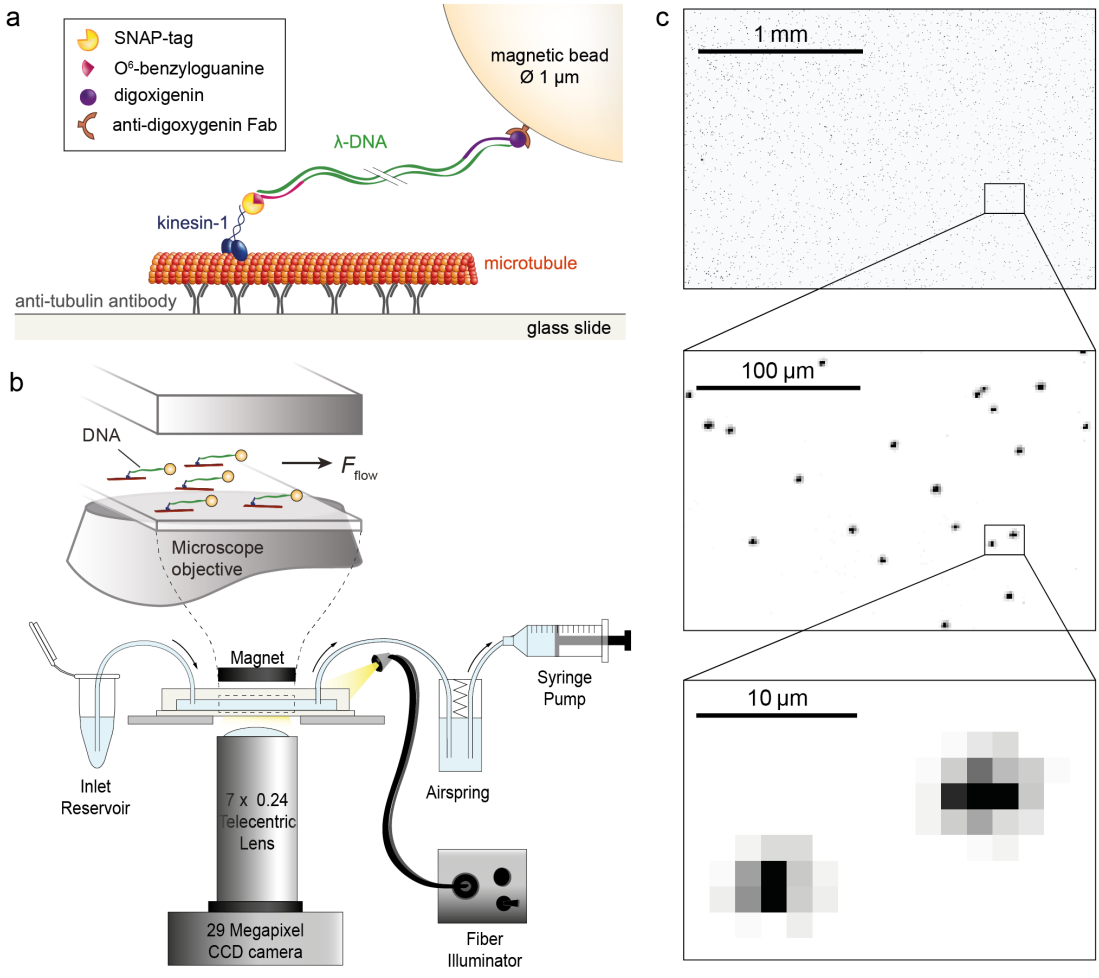

Figure 1. Kinesin-1 microfluidics-based force assay. (a) Molecular details of attaching a 1-µm sized paramagnetic bead to an individual kinesin-1 motor via a long, double-stranded DNA linker. (b) Schematic overview of the experimental setup. Inset presents a side view of the interior of the flow cell (not to scale). The direction of applied force is indicated by the arrow. (c) Dark-field microscopy images of multiple magnetic beads (up to 30,000 beads per field-of-view) tethered to individual kinesin-1 motors. The top panel represents only 23 % of the full field-of-view.

In situ force calibration. As routinely used in the field of magnetic tweezers, we used the fluctuations of the tethered beads in the direction transverse to the flow for an in situ calibration of the acting forces[27]. By relating the energy of a Hookean spring to the equipartition theorem the following equation is obtained:

$$\langle \delta y^2 \rangle = \frac{k_B T l}{F}. \quad (1)$$

The mean-square displacement of a bead in the transverse direction $<\delta y^2>$, together with the length of the tether l, temperature T and Boltzmann constant k_B are sufficient to determine the force F pulling on the molecule. To enable precise determination of the tether extension for each molecule, we coupled the force-extension relation for dsDNA[28] with equation (1) and solved the set of these two equations numerically to obtain both tether extension and force magnitude for each molecule individually (see Methods for details, including a correction for motion blurring caused by the finite camera integration time).

The measured magnitude of the fluctuations of individual beads decreased with increasing flow rate (Figure 2a). Using the trajectories from all beads which exhibited unidirectional movement after the addition of ATP, we determined a characteristic force for each experiment. Figure 2b presents the force distributions for exemplary experiments performed at flow rates of 10, 20, 30 and 40 µl min^{-1}. The median forces in the presented experiments were 1.1, 1.6, 1.9 and 2.5 pN, respectively. The broad distribution of estimated forces can be attributed to local flow instabilities, as well as to a potential non-uniformity of bead sizes. The influence of the latter could, in the future, be assessed by bead sizing using convolution and correlation image analysis[29].

Motility of individual kinesin-1 motors under resisting and assisting loads. After AMPPNP had been washed out by ATP-containing buffer the motors started to translocate (Supplementary Figure 1), predominantly along the flow axis as the majority of the microtubules were aligned by the flow (Supplementary Figure 3). We discriminated between different stepping directions by looking at the bead displacement in the *x*-*y* plane. Exemplary

trajectories of kinesin-1 motors moving against the flow (i.e. experiencing a resisting load) and with the flow (i.e. experiencing an assisting load) are presented in Figures 3a and 3b, respectively.

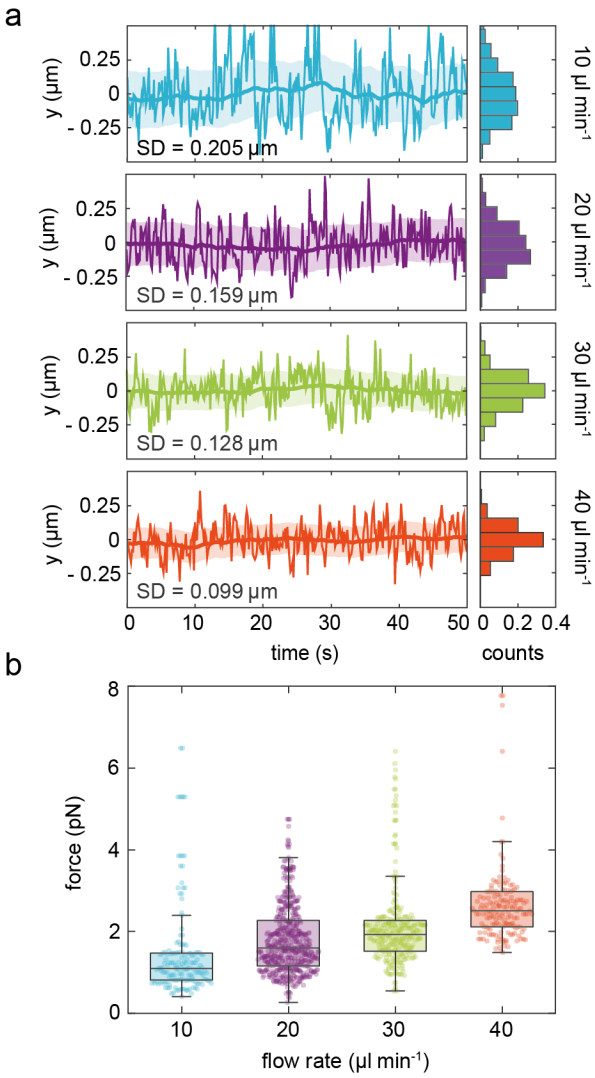

Figure 2. Fluctuation-based in situ force calibration. (a) Bead fluctuations in the direction *y* transverse to the flow over time for flow rates of 10, 20, 30 and 40 µl min^{-1}. Histograms on the right-hand side present relative occurrences of *y* positions. (b) Distributions of estimated forces for the different flow rates. The forces were estimated based on the bead fluctuations displayed in a. Boxes extend from 25th to 75th percentiles, with a line at the median. Whiskers span 1.5× interquartile range. Colored dots represent individual beads (n = 162, 553, 285, 169).

Although the microtubule axes were mostly aligned with the flow direction, their polarities (i.e. the positions of their plus and minus ends) were arbitrary (Supplementary Figure 3). Therefore, we were able to investigate the motility of individual plus-end directed kinesin-1 motors under resisting and assisting loads of the same magnitude simultaneously. Velocity

histograms from a single experiment with 444 motility events against the flow and 476 motility events with the flow are presented in Figures 3c and 3d. Under a median load of 1.6 pN in the presented experiment, the kinesin-1 motors stepped with mean velocities of 0.423 ± 0.008 μm s^{-1} against the flow and 0.557 ± 0.014 μm s^{-1} (mean ± SEM) with the flow.

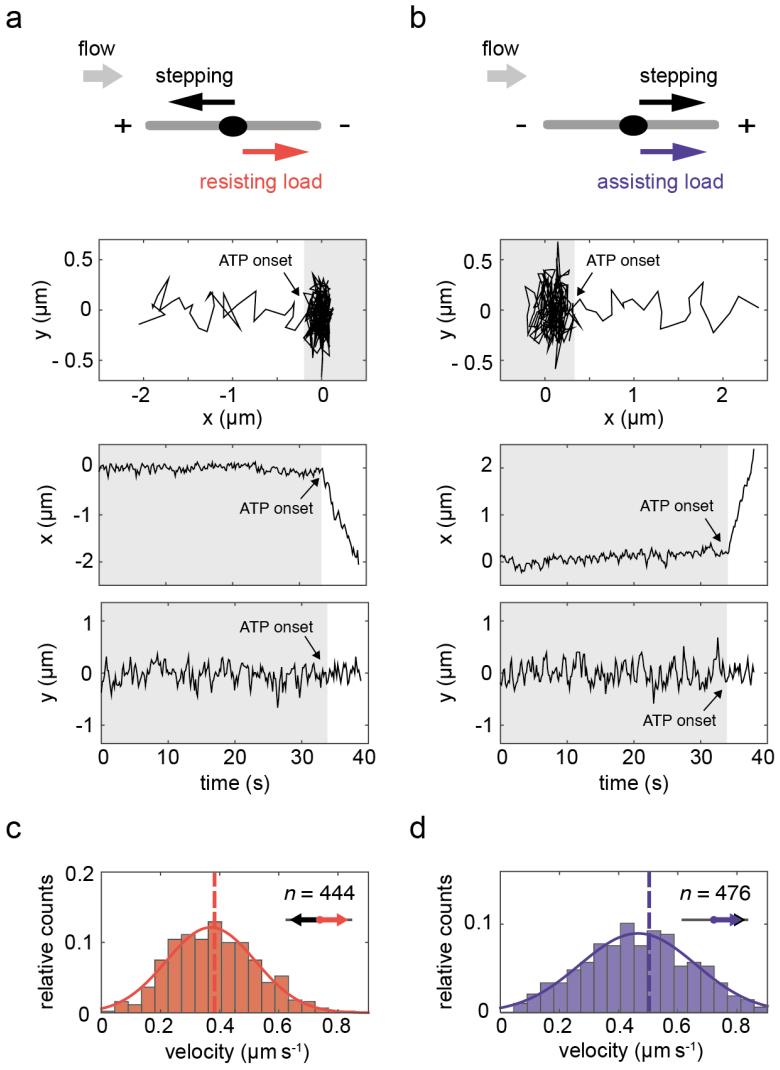

Figure 3. Single-molecule motility events under resisting and assisting load. (a) Setup and exemplary trajectory of a motor stepping against the flow (towards decreasing *x*-position, corresponding to a resisting load). The plots from top to bottom present: the position of the bead in a 2D plane over 40 seconds before detachment, the *x*-position over time and *y*-position over time. The gray-shaded areas correspond to the period before ATP onset, i.e. the time when the motors were still arrested in the presence of AMPPNP. (b) Analogous setup and exemplary trajectory of a motor stepping with the flow (towards increasing *x*-position, corresponding to an assisting load). (c) Velocity histogram of 444 stepping events under resisting load. (d) Velocity histogram of 476 stepping events under assisting load. In c and d, overlays of Gaussian fits are presented and vertical dashed lines represent mean velocity values.

Kinesin-1 force-velocity curve. By varying the flow rates, we applied loads of different magnitudes and constructed a force-velocity curve for kinesin-1 (Figure 4a). Since the distribution of forces acting on the molecules under a given flow rate is considerably broad (Figure 2b), we assigned force loads to each stepping event individually and compared velocities for the data grouped according to the estimated values into 0.3-pN wide bins. We observe that with increasing resisting load the stepping velocity of kinesin-1 progressively decreased. It reached a mean value of 0.532 ± 0.025 μm s^{-1} (mean ± SEM) for the lowest load bin (0.9 ± 0.15 pN) and 0.266 ± 0.016 μm s^{-1} for the highest load bin (3 ± 0.15 pN). Under conditions of assisting load, we found the highest velocity of 0.686 ± 0.038 μm s^{-1} for the lowest load bin.

With increasing assisting load, the kinesin-1 stepping velocity slightly decreased and reached a mean value of 0.441 ± 0.037 μm s^{-1} for the highest load bin. The force-velocity curve obtained for kinesin-1 in our study follows qualitatively[30] and even quantitatively[27] earlier data from optical tweezers, as well as from force-fiber[32] measurements for resisting loads (Figure 4d). We note, that contrary to the data reported in Ref. [30,31] but consistent with trend of the data reported in Ref. [27] the velocity observed in our experiments showed a marked decrease under increasing assisting loads.

Dependence of further motility parameters on applied force. Apart from velocity, we were also able to readily evaluate the run lengths and interaction times of individual kinesin-1 motors under the different loads (Figure 4b–c). To account for under-representation of very short stepping events, we estimated these two parameters using least-squares fitting of the cumulative distribution function with free cut-off parameters[33]. The measured run lengths appeared fairly constant for loads between –2.7 pN and 2.1 pN, with a mean at 0.62 μm (Figure 4b). For assisting loads larger than 2.7 pN and resisting loads larger than 2.1 pN the run lengths decreased. This is in contrast to observations made in conventional optical tweezers experiments, where the measured run lengths decreased already drastically for moderate loads,

e.g. showing a three-fold decrease at 2 pN resisting load[34]. This discrepancy can be attributed to the high vertical forces in conventional optical tweezers experiments that cause pre-mature detachment of motors compared to forces applied more horizontally[35–37]. The mean run-length value of 0.62 µm observed at low loads, corresponds well to the previously observed value of 0.67 µm for unloaded motors[33].

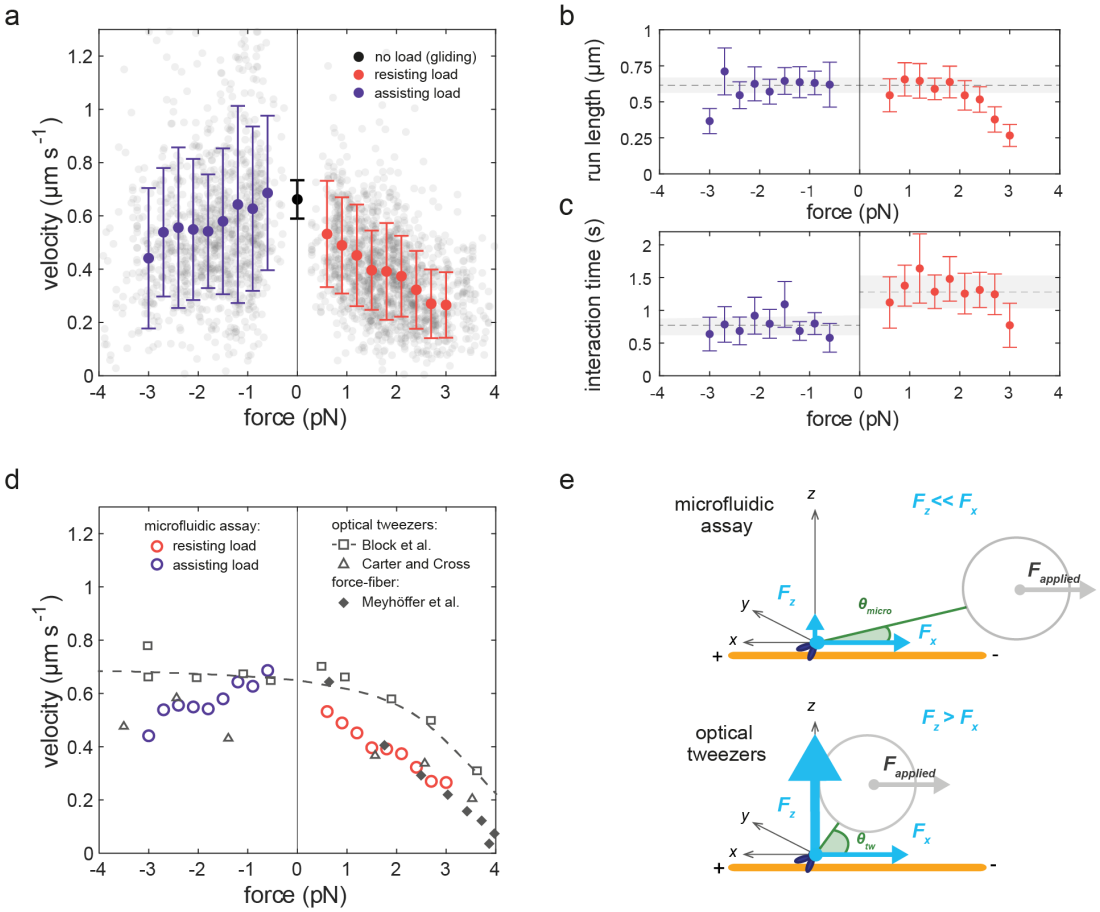

Figure 4. Force-dependence of motility parameters for kinesin-1 as probed by the microfluidic assay. (a) Stepping velocity of kinesin-1 observed under assisting (violet dots) and resisting (red dots) loads of different magnitudes. Plotted values represent means ± SD of velocity data contained within 0.3-pN force bin (n = 52–213 per bin). Gray scatter represents individual events used for binning (n = 2484, data pooled from measurements performed at 10 – 50 µl min^{-1}). The black dot represents the velocity of the kinesin-1 motor used in this study under no load condition as evaluated by gliding assays (mean ± SD, see Supplementary Figure 4). (b,c) Force dependence of run lengths and interaction times for events in (a), plotted values represent means ± 2×SD obtained from bootstrapping. As guides for the eye, means of bins -2.7 to 2.1 pN for run length, and mean of all assisting as well as all resisting load bins for interaction time, are indicated with the dashed gray line. Shaded areas represent SD. (d) Overlay of force-velocity data from our study (open circles) with data obtained in optical tweezers' studies by Block et al.[30] (open squares and dashed curve showing the fit of a five-step model) and by Carter and Cross[31] (open triangles), and in a force-fiber assay by Meyhöfer et al.[32] (filled diamonds). (e) Comparison of experimental geometries in the microfluidic assay presented in

this study (upper scheme) and in a conventional optical tweezers experiment (lower scheme). θ - inclination angle between the microtubule and the tether in the case of the microfluidic setup (θ_{micro}) and a conventional optical tweezer configuration (θ_{tw}); $F_{applied}$ – force applied on the bead; F_z – vectorial component of the force pointing in the z direction (vertical force); F_x - vectorial component of the force pointing in the x direction (horizontal force).

The measured interaction times appeared fairly constant for all applied assisting loads, with a mean at 0.77 s (Figure 4c). For resisting loads the interaction times appeared constant, with a mean at 1.28 s, up to 2.7 pN before decreasing above that load. The overall higher interaction times observed under resisting loads, as compared to assisting loads, suggest that kinesin-1 exhibits a higher detachment rate under assisting loads. This is in agreement with the higher unbinding force observed for kinesin-1 under resisting load as compared to assisting load[38] and with the theoretical prediction that horizontal forces alone, as predominantly present in our setup, decelerate motor detachment[35,36]. The mean interaction times obtained for both assisting and resisting loads, correspond well to the interaction time of 0.95 s under unloaded conditions reported previously for the kinesin-1 at room temperature[33]. The good agreements of both run lengths and interaction times with previously reported and predicted values for single kinesin-1 motors ascertains that we evaluated the stepping of single molecules.

Reducing the vertical force component. Our hydrodynamic force assay not only enables parallelization of the measurements on cytoskeletal motors, but also provides an alternative geometry of force application compared to existing methods. While optical traps—the method of choice for characterizing cytoskeletal motors—have been exploited to study the application of forward, backward[31,34,39], and sideward loads[30,40] on stepping kinesins using a variety of geometries[41,42], they generally suffer from a poor control over vertically applied forces, which may bias the measurements performed[43–46]. Although the force is applied horizontally onto the bead in a conventional optical trap experiment, the molecule under investigation is experiencing a vertical load which, in fact, can surpass the applied horizontal force in magnitude[43]. Such substantial vertical load is pulling the motor away from the filament and can influence its

detachment rate[35–37,43,46]. In our approach, the introduction of a spacer between the motor and the bead reduces the vertical force component to less than 15% of the applied force (see Figure 4e and Supplementary Table 1), thus applying forces more stringently in the direction of motor movement. Such a prolonged spacer could, in principle, be implemented in conventional optical tweezer experiments. A reduction of vertical force component in optical tweezers can also be achieved in a three-bead assay with suspended microtubules, as recently demonstrated[37]. To explore the influence of loading geometry on the measured motility parameters in our assay, experiments with varying linker length or varying vertical magnetic force could be performed. The different loading scenarios may reflect the physiological transport of cargos differing in size and shape inside the cell, or differently positioned motors in multi-motor assemblies present in vivo.

Method performance and additional assets. Optimal performance of our method is achieved at intermediate forces. At very low forces (< 0.5 pN) the bead fluctuations limit the accuracy of the velocity measurements. At high forces, in turn, the observation time is limited due to the decreased processivity of the motor. However, the latter is specific to single kinesin-1 motors, exhibiting a force-dependent run length[34], and will likely not be an issue for other mechanosystems, such as dynein[47,48] or multi-motor transport systems[49].

An additional asset of our method is the possibility to study the motor velocity in an angle-resolved manner (see Supplementary Figure 5). Depending on the alignment of the microtubules with respect to the flow direction, some motors will step not directly against or with the direction of applied force. In this study, the microtubules were aligned with the long flow cell axis to maximize the number of events stepping parallel to the force direction (Supplementary Figure 3), however, the orientation of the microtubules can be randomized by applying a perpendicular or turbulent flow while introducing microtubules to the flow cell.

The straightforward in situ force calibration and the flexibility of the assay geometry design due to adjustable DNA tether length and possibility to manipulate the bead height by changing

the magnetic force, further enhance the appeal of the presented method. Finally, we note that our approach can be implemented using any standard wide-field microscope at low cost.

Conclusions

Single-molecule manipulation techniques have shed light on the functioning principles of many molecular machines in the cell. Yet, their widespread applicability and utilization for single-molecule screening purposes is limited by the lack of robust high-throughput technologies. Our versatile, massively multiplexed microfluidic assay for the application of forces to molecular mechanosystems, such as stepping cytoskeletal motors and motor complexes, presents a leap towards wider usage of single-molecule approaches. We envision a broad implementation of the assay in fundamental research of biological systems as well as in medical diagnostics applications, where rapid acquisition of population-wide data is of key importance.

Methods

Protein production and purification. We used a truncated kinesin-1 heavy chain from *Rattus norvegicus* (1-430 aa) fused to a SNAP-tag and 8xHis-tag (rKin430-SNAP-8xHis in a pET17b, see Supplementary Figure 6 for full protein sequence). The SNAP-tag allows for covalent binding of O6-benzylguanine (BG) to the protein[50]. Protein expression was performed in *Escherichia coli* BL21(DE3) pRARE (Invitrogen) under T7 promoter with 1 mM isopropyl-β-D-thiogalactopyranoside (IPTG) induction at OD600 = 0.6 for 14 h at 18 °C. After protein expression, bacterial cells were disrupted in a high-pressure homogenizer (Emulsiflex-C3, Avestin Inc) in the presence of protease inhibitors (Protease Inhibitor Cocktail Tablets, Roche Diagnostics GmbH). Crude lysate was centrifuged at 20,000g at 4°C. The supernatant was loaded on a HisTrapTM metal affinity column (GE Healthcare Life Sciences). All protein purification steps were performed in buffers based on 2 x PBS (274 mM NaCl, 5.4 mM KCl, 16.2 mM Na_2HPO_4 $2H_2O$, 3.52 mM KH_2PO_4, 2 mM $MgCl_2$, pH 7.4) containing 1 mM ATP and 1 mM DTT. Column washing was performed with 10 times the column volume of: 5 mM ATP in 2 x PBS, 6 x PBS, 15 mM and 30 mM imidazole in 2 x PBS; followed by elution with 500 mM imidazole in 2 x PBS. Size and purity of the protein after elution was checked by SDS–PAGE (Supplementary Figure 7). The peak fractions were then desalted on size-exclusion Sephadex columns (NAP25 gravity column, GE Healthcare). Collected protein was snap-frozen in liquid nitrogen and stored at -80°C. To check the activity of the obtained protein, gliding motility assays were performed with specific immobilization of motors on the surface via penta-His antibodies (34660, Qiagen) as previously described[51] (Supplementary Figure 4). Microtubule movement was tracked using FIESTA software[52]. On basis of Gaussian fitting the mean gliding velocity for KinSNAP was estimated to be 662 ± 72 nm s^{-1} (mean ± SD; n = 243). This velocity corresponds well to literature data as the microtubule gliding velocity at saturating ATP concentrations and pH 6.9 is reported to fall between 500 and 750 nm s^{-1} [53].

Microtubule polymerization. Microtubules stabilized with guanosine-5'-[αβ-methyleno] triphosphate (GMPCPP; Jena Bioscience, Germany) were prepared by polymerization of in-house prepared porcine tubulin labelled partially with rhodamine (1:3 ratio of labelled to unlabeled tubulin). Polymerization was carried out using 0.25 mg ml^{-1} tubulin in BRB80 buffer (80 mM piperazine-N,N'-bis(2-ethanesulfonic acid) (PIPES), 1 mM $MgCl_2$, 1 mM ethylene glycol tetraacetic acid (EGTA), pH 6.9 adjusted with KOH) supplemented with additional $MgCl_2$ to final concentration of 4 mM and 1 mM GMPCPP. The polymerization reaction was pre-incubated for 10 min on ice and continued for 2 h at 37ºC. Afterwards, to remove unpolymerized tubulin dimers from the solution, the microtubules were spun down in a tabletop microcentrifuge (Heraeus Fresco 17, Thermo Scientific Inc.) at 17000 g for 15 minutes and resuspend in 250 µl of BRB80 buffer.

Preparation of doubly-functionalized DNA linkers. λ-DNA (N3011, NEB) was functionalized on one end with O^6-benzylguanine (BG) and on the other with digoxigenin (Dig) by two-step ligation of oligonucleotides with functional groups to the λ-DNA overhangs. The Dig-oligonucleotide was purchased in functionalized form ($AGGTCGCCGCCCA_{12}$-Dig, Eurofins MWG Operon). The BG-oligonucleotide was prepared by coupling of 10 mM BG–GLA–NHS (S9151, NEB) to 0.33 mM amine-functionalized oligonucleotide ($GGGCGGCGACCT-NH_2$, Eurofins MWG Operon). The coupling reaction was conducted in 67 mM HEPES (pH 8.5) and 50% DMSO for 30 min at room temperature. The uncoupled BG-GLA-NHS was removed by filtration on Micro Bio-Spin™ P-6 Gel Columns (Bio-Rad).

The BG-oligonucleotide (210 nM) was ligated to the 3' end of the λ-DNA (3 nM) in 500 µl T4 ligase buffer (50 mM Tris-HCl, 10 mM $MgCl_2$, 1 mM ATP and 10 mM DTT, pH 7.5, NEB). Before adding the ligase, the solution was incubated for 5 min at 65ºC and cooled down slowly to allow for annealing. For the ligation 800 units of T4 DNA ligase (NEB) were added and the reaction was held overnight at room temperature. Next, Dig-oligonucleotide (460 nM, a 3-fold excess with respect to BG-oligonucleotide) was annealed to the 5' end of the λ-DNA by

incubating at 45ºC for 30 min. After cooling the solution down to room temperature, additional 800 units of T4 DNA ligase were supplemented and the ligation reaction was held for 2 h at room temperature. To get rid of the remaining oligonucleotides and oligonucleotide duplexes, the ligation product was dialyzed at 4ºC against 0.5 l TE buffer (50 mM Tris-HCl, 1 mM EDTA) using 1 ml Float-A-Lyzer G2 Dialysis Device with molecular cutoff of 1000 kDa (G235037, Spectrum Labs). The dialysis buffer was exchanged 5 times with 4-16 h intervals.

Bead functionalization. Superparamagnetic polystyrene beads with a diameter of 1.08 µm (Dynabeads MyOne™ Tosylactivated, Invitrogen) were functionalized via an amine coupling reaction with 20 µg of anti-digoxigenin Fab fragments (Invitrogen) per mg of beads according to a protocol described elsewhere[54].

Coverslip functionalization. For making their surface hydrophobic, the coverslips used for all experiments were coated with DDS (dichlorodimethylsilane) prior to use. DDS-functionalization involves several cleaning steps, including 60 min incubation in Piranha solution (30% H_2O_2 and 70% H_2SO_4) and a silanization step using DDS diluted in TCE (trichloroethylene). Details can be found elsewhere[55].

Flow cell assembly. For performing the microfluidic assays, a PDMS slab with 3 mm wide and 100 µm high channel was placed on the DDS-functionalized coverslip and pressed with a custom-made metal frame to avoid leakage. Flow channels terminate with Y junctions at each end providing for two inlets and two outlets. The solutions were introduced to the flow cell by a pump (AL-200, WPI, Inc) operated in withdrawal mode through polyethylene tubing (PE-60, 0.76 mm inner and 1.22 mm outer diameter) inserted into 1.2 mm holes punched into the PDMS. Volumetric flow rates of 10, 20, 30, 40 or 50 µl min^{-1} (corresponding to calculated average flow velocities of 0.6, 1.1, 1.7, 2.2 or 2.8 mm s^{-1}) were kept constant during the measurements. For the flow cell dimensions and flow velocities used the flow is laminar ($Re < 1$, see Supplementary Table 2).

On-surface assay assembly. Anti-β-tubulin antibodies (75 μg ml^{-1}, SAP.4G5, Sigma-Aldrich) in BRB80 was flushed into the flow cell and incubated for 5 min to allow for hydrophobic interaction-based absorption to the surface. Next, the channel surface was passivated with 1% Pluronic F127 (P2443, Sigma-Aldrich) in BRB80 for 30-60 min. The flow cell was then mounted on the imaging setup and connected to the syringe pump operated at 20 μl min^{-1} throughout the following assembly steps. First, the flow cell was washed with 200 μl of BRB80 solution. Next, 250 μl of GMPCPP-stabilized microtubule solution in BRB80 was flowed through the channel. SNAP-tagged kinesin-1 (11 nM) was pre-coupled to the functionalized DNA linker (0.4 nM) by incubation for 2 to 3 h at room temperature on a rotary mixer and diluted 1:10 in imaging solution (0.2 mg ml^{-1} casein, 10 mM DDT, 0.1% Tween 20 in BRB80) containing 100 μM adenylyl-imidodiphosphate (AMPPNP). 200 μl of so-prepared kinesin-DNA complexes was introduced to the channel. After a subsequent wash with 200 μl of imaging solution, anti-digoxigenin beads were flowed through the flow cell and attached on the fly to the kinesin-bound DNA linkers. Subsequently, another washing step was performed to remove the unbound beads from the flow cell. During this step the flow rate was adjusted to the desired value (between 10 and 50 μl min^{-1}) and a magnet was placed at a defined height above the flow cell to minimize interaction of the tethered beads with the surface. Finally, to initiate kinesin stepping, an imaging solution containing 10 mM ATP was flowed into the flow cell at the respective flow rate.

Imaging setup and data acquisition. A fiber illuminator (Thorlabs) was used to illuminate the flow cell from the side. The light scattered by the beads was collected through a telocentric lens (TL12K-70-15, Lensation) with 7x magnification mounted directly on top of a 29 Megapixel CCD camera (Prosilica GX6600, Allied Vision Technologies, 5.5 μm pixel size). Images were collected at 150 ms per frame continuously in streaming mode using StreamPix imaging software (NorPix). All the experiments were performed at room temperature (~23°C).

Data analysis. The centroid of the beads was tracked using a custom ImageJ plugin programmed in house, the core of the tracking algorithm corresponds to the *Peak Tracker* (https://duderstadt-lab.github.io/mars-docs/docs/image/PeakTracker/) implemented in the open-source **M**olecular **Ar**chive **S**uite, *mars*, software (https://github.com/duderstadt-lab/mars-core). Bead trajectories were corrected for drift by subtracting an averaged trace of several immobile particles. For the velocity calculations, the distance along the line fitted to the *x*-*y* displacement of the bead and time were used. The start and end times of the stepping events were marked by hand.

Localization precision. To determine the localization precision for bead tracking, we estimated the standard deviation of *x* and *y* positions for 12 beads stuck to the surface over the time of 5 min. The used traces were corrected for drift by subtracting the average of all stuck bead traces. The obtained standard deviations averaged at 32 nm for both *x* and *y*. This value corresponds to the experimental value of localization precision, the theoretical limit of the tracking precision in the used configuration was previously calculated to be 6 nm[26].

Estimation of the acting force. In our system a bead is tethered with a dsDNA tether with extension length l to the kinesin-1 motor attached to the microtubules on a glass slide (Supplementary Figure 8a). The fluctuations of the bead in the direction perpendicular to the flow, y, can be approximated by the movement of a pendulum with a length corresponding to the extension of the tether l (Supplementary Figure 8b,c). During the stochastic movement of the bead, the force F_{spring} is pushing it back to the equilibrium state and is defined as:

$$F_{spring} = Fsin(\delta\varphi), \tag{1}$$

where F is the applied drag force and $\delta\varphi$ is the angle between F and the tether (Supplementary Figure 8c).

For small angles $sin(\delta\varphi)$, can be approximated as $\frac{\delta y}{l}$ and the above equation takes form:

$$F_{spring} = F\frac{\delta y}{l}. \tag{2}$$

Therefore, in our Hookean system the spring constant defining the stiffness is described as:

$$k_y = \frac{F}{l}. \tag{3}$$

The mean energy of a Hookean system is expressed as follows:

$$\langle E \rangle = \frac{1}{2} k_y \langle \delta y^2 \rangle. \tag{4}$$

Relating this equation to the equipartition theorem yields:

$$\frac{1}{2} k_B T = \frac{1}{2} k_y \langle \delta y^2 \rangle, \tag{5}$$

where k_B is the Boltzmann constant and T is the temperature. We can therefore relate the force F to the root-mean-square deviation of position in y in the following way:

$$\langle \delta y^2 \rangle = \frac{k_B T}{k_y} = \frac{k_B T l}{F}. \tag{6}$$

Similar approaches were used for force estimation in previous studies using magnetic tweezers[27], as well as microfluidic DNA stretching[21].

For estimating the bead fluctuations, only trajectories with subsequent stepping events were considered. For each trajectory a fragment of a minimum of 100 data points of the position in the y direction was chosen. These fragments were visually inspected to discard trajectory regions where abrupt position changes or loss of fluctuations due to sticking of the bead to the surface were present. The measured mean square displacement of the bead position in y, $\langle \delta y^2 \rangle_m$, was estimated according to the formula:

$$\langle \delta y^2 \rangle_m = \langle y^2 \rangle - \langle y \rangle^2, \tag{7}$$

and corrected for motion blurring caused by the finite camera integration time W, in our case equal to 150 ms, using a correction function $S(\alpha)$[56] as follows:

$$\langle \delta y^2 \rangle = \frac{\langle \delta y^2 \rangle_m}{S(\alpha)}. \tag{8}$$

The correction function $S(\alpha)$ is given by[56]:

$$S(\alpha) = \frac{2}{\alpha} - \frac{2}{\alpha^2}(1 - \exp(-\alpha)), \tag{9}$$

where α is the ratio of the camera integration time W to the trap relaxation time τ

$$\alpha \equiv \frac{W}{\tau}, \tag{10}$$

with $\tau = \frac{\gamma}{k_y}$, where k_y is the spring constant of the trap (Eq. 3), and γ the friction coefficient of the particle defined by the Stoke's formula $\gamma = 6\pi\eta R$, where η represents dynamic viscosity of the medium and R the radius of the bead. Hence, α can be expressed as:

$$\alpha = \frac{FW}{l\ 6\pi\eta R}. \tag{11}$$

Since W, η, and R are constant and dictated by the experimental conditions, α becomes a function of the applied drag force F and the extension of the tether l.

Taking into account the motion blurring correction, Eq. 6 can be rewritten as:

$$\frac{\langle \delta y^2 \rangle_m}{S(\alpha)} = \frac{k_B T l}{F}. \tag{12}$$

Since we do not experimentally verify the tether extension l and, having two variables F and l, we cannot estimate the force solely using Eq. 12. We therefore took advantage of the force-extension relation that describes the behavior of a DNA strand when pulled by a force[28]:

$$\frac{FP}{k_B T} = \frac{1}{4}\left(1 - \frac{l}{l_0}\right)^{-2} - \frac{1}{4} + \frac{l}{l_0} \tag{13}$$

with l_0 corresponding to the contour length of the λ-DNA (16.2 μm) and P to the persistence length of double stranded DNA[28](50 nm), to create a set of equations (Eq. 12 and 13). The obtained set of two polynomial equations cannot be solved analytically; therefore we employed a numerical solver to obtain the values of F and l for each measured molecule (*vpasolve* function in MATLAB R2018b, The MathWorks, Inc., Natick, Massachusetts, United States).

Associated Content

The following Supporting Information is available alongside the manuscript.

Supplementary Information: Supplementary Figures 1–8 and Supplementary Tables 1– 2 (PDF)

Author Contributions

S.D., A.M.O. and W.J.W. conceived the project. M.U., with support of A.L., W.J.W. and K.E.D. performed the experiments. W.J.W. cloned and expressed the SNAP-tagged kinesin-1 protein. M.U. and K.E.D. wrote the analysis software. M.U. analyzed the data, prepared figures and wrote the original version of the manuscript. All authors revised and edited the manuscript. S.D., K.E.D., A.M.O. and W.J.W. supervised the project. S.D. and K.E.D. acquired funding.

Acknowledgement

We thank Corina Bräuer and Cornelia Thodte for technical assistance, Felix Ruhnow and Erik Schäffer for fruitful discussions, Lucas Wittwer and Sebastian Aland for help with theoretical considerations regarding bead position, and Georg Krainer for helpful suggestions on the manuscript. We acknowledge financial support from the Dresden International Graduate School for Biomedicine and Bioengineering (DIGS-BB, stipend to A.L.), the German Excellence Initiative (TU Dresden Support-the-Best grant to S.D.), the Human Frontier Science Program (Long-term fellowship LT000180/2012-L to K.E.D.), and support from the Max Planck Society to K.E.D.

References

1. Bustamante, C., Macosko, J. C. & Wuite, G. J. Grabbing the cat by the tail: manipulating molecules one by one. *Nat. Rev. Mol. Cell Biol.* **1**, 130–6 (2000).

2. Clausen-Schaumann, H., Seitz, M., Krautbauer, R. & Gaub, H. E. Force spectroscopy with single bio-molecules. *Curr. Opin. Chem. Biol.* **4**, 524–530 (2000).

3. Neuman, K. C. & Nagy, A. Single-molecule force spectroscopy: optical tweezers, magnetic tweezers and atomic force microscopy. *Nat. Methods* **5**, 491–505 (2008).

4. de Souza, N. Pulling on single molecules. *Nat. Methods* **9**, 873–877 (2012).

5. Alsteens, D., Tay, S. & Müller, D. J. Toward high-throughput biomechanical phenotyping of single molecules. *Nat. Publ. Gr.* **12**, 45–46 (2015).

6. Emiliani, V., Sanvitto, D., Zahid, M., Gerbal, F. & Coppey-Moisan, M. Multi force optical tweezers to generate gradients of forces. *Opt. Express* **12**, 3906–3910 (2004).

7. Soltani, M. *et al*. Nanophotonic trapping for precise manipulation of biomolecular arrays. *Nat. Nanotechnol.* **9**, 448–52 (2014).

8. Tanaka, Y. & Wakida, S. Time-shared optical tweezers with a microlens array for dynamic microbead arrays. *Biomed. Opt. Express* **6**, 3670 (2015).

9. De Vlaminck, I. & Dekker, C. Recent Advances in Magnetic Tweezers. *Annu. Rev. Biophys.* **41**, 453–472 (2012).

10. Kriegel, F. *et al*. Probing the salt dependence of the torsional stiffness of DNA by multiplexed magnetic torque tweezers. *Nucleic Acids Res.* **45**, 5920–5929 (2017).

11. Santos, Á., Fili, N., Pearson, D. S., Hari-gupta, Y. & Christopher, P. High throughput mechanobiology: Force modulation of ensemble biochemical and cell-based assays.

bioRxiv 10.1101/2020.05.05.065912 (2020) doi:10.1101/2020.05.05.065912.

12. JPK Instruments AG. Single molecule force spectroscopy with the ForceRobot® 300. http://usa.jpk.com/index.231.us.html.

13. Otten, M. *et al*. From genes to protein mechanics on a chip. *Nat. Methods* **11**, 1–7 (2014).

14. Halvorsen, K. & Wong, W. P. Massively parallel single-molecule manipulation using centrifugal force. *Biophys. J.* **98**, L53–L55 (2010).

15. Yang, D., Ward, A., Halvorsen, K. & Wong, W. P. Multiplexed single-molecule force spectroscopy using a centrifuge. *Nat. Commun.* **7**, 1–7 (2016).

16. Sitters, G. *et al*. Acoustic force spectroscopy. *Nat. Methods* **12**, 47–50 (2015).

17. Zocchi, G. Proteins unfold in steps. *Proc. Natl. Acad. Sci. U. S. A.* **94**, 10647–10651 (1997).

18. Zocchi, G. Force measurements on single molecular contacts through evanescent wave microscopy. *Biophys. J.* **81**, 2946–2953 (2001).

19. Türkcan, S., Richly, M. U., Bouzigues, C. I., Allain, J.-M. & Alexandrou, A. Receptor displacement in the cell membrane by hydrodynamic force amplification through nanoparticles. *Biophys. J.* **105**, 116–26 (2013).

20. Yokokawa, R., Sakai, Y., Okonogi, A., Kanno, I. & Kotera, H. Measuring the force of adhesion between multiple kinesins and a microtubule using the fluid force produced by microfluidic flow. *Microfluid. Nanofluidics* **11**, 519–527 (2011).

21. Oijen, A. M. Van, Blainey, P. C. & Crampton, D. J. Single-Molecule Kinetics of Exonuclease Reveal Base Dependence. *Science (80-.).* 1235–1238 (2003).

22. Lee, J. B. *et al*. DNA primase acts as a molecular brake in DNA replication. *Nature* **439**,

621–624 (2006).

23. Kim, S., Blainey, P. C., Schroeder, C. M. & Xie, X. S. Multiplexed single-molecule assay for enzymatic activity on flow-stretched DNA. *Nat. Methods* **4**, 397–399 (2007).

24. Tanner, N. A. *et al*. Single-molecule studies of fork dynamics in Escherichia coli DNA replication. *Nat. Struct. Mol. Biol.* **15**, 170–176 (2008).

25. Duderstadt, K. E. *et al*. Simultaneous Real-Time Imaging of Leading and Lagging Strand Synthesis Reveals the Coordination Dynamics of Single Replisomes. *Mol. Cell* **64**, 1035–1047 (2016).

26. Agarwal, R. & Duderstadt, K. E. Multiplex flow magnetic tweezers reveal rare enzymatic events with single molecule precision. *Nat. Commun.* **11**, (2020).

27. Strick, T. R., Allemand, J. F., Bensimon, D. & Croquette, V. Behavior of supercoiled DNA. *Biophys. J.* **74**, 2016–28 (1998).

28. Bustamante, C., Marko, J. F., Siggia, E. D. & Smith, S. Entropic Elasticity of λ-Phage DNA. *Science (80-.).* **265**, 1599–1600 (1994).

29. Gennerich, A. & Schild, D. Sizing-up finite fluorescent particles with nanometer-scale precision by convolution and correlation image analysis. *Eur. Biophys. J.* **34**, 181–199 (2005).

30. Block, S. M., Asbury, C. L., Shaevitz, J. W. & Lang, M. J. Probing the kinesin reaction cycle with a 2D optical force clamp. *Proc. Natl. Acad. Sci. U. S. A.* **100**, 2351–6 (2003).

31. Carter, N. J. & Cross, R. a. Mechanics of the kinesin step. *Nature* **435**, 308–12 (2005).

32. Meyhöfer, E. & Howard, J. The force generated by a single kinesin molecule against an elastic load. *Proc. Natl. Acad. Sci. U. S. A.* **92**, 574–8 (1995).

33. Ruhnow, F., Kloβ, L. & Diez, S. Challenges in Estimating the Motility Parameters of Single Processive Motor Proteins. *Biophys. J.* **113**, 2433–2443 (2017).

34. Schnitzer, M. J., Visscher, K. & Block, S. M. Force production by single kinesin motors. *Nat. Cell Biol.* **2**, 718–23 (2000).

35. Khataee, H. & Howard, J. Force Generated by Two Kinesin Motors Depends on the Load Direction and Intermolecular Coupling. *Phys. Rev. Lett.* **122**, 188101 (2019).

36. Khataee, H., Mahamdeh, M. & Neufeld, Z. Processivity of molecular motors under vectorial loads. *Phys. Rev. E* **102**, 1–6 (2020).

37. Pyrpassopoulos, S., Shuman, H. & Ostap, E. M. Modulation of Kinesin's Load-Bearing Capacity by Force Geometry and the Microtubule Track. *Biophys. J.* **118**, 243–253 (2019).

38. Uemura, S. *et al*. Kinesin-microtubule binding depends on both nucleotide state and loading direction. *Proc. Natl. Acad. Sci.* **99**, 5977–5981 (2002).

39. Nishiyama, M., Higuchi, H. & Yanagida, T. Chemomechanical coupling of the forward and backward steps of single kinesin molecules. *Nat. Cell Biol.* **4**, 790–7 (2002).

40. Lang, M. J., Asbury, C. L., Shaevitz, J. W. & Block, S. M. An automated two-dimensional optical force clamp for single molecule studies. *Biophys. J.* **83**, 491–501 (2002).

41. Bugiel, M., Böhl, E. & Schäffer, E. The kinesin-8 Kip3 switches protofilaments in a sideward random walk asymmetrically biased by force. *Biophys. J.* **108**, 2019–2027 (2015).

42. Bugiel, M., Mitra, A., Girardo, S., Diez, S. & Schäffer, E. Measuring Microtubule Supertwist and Defects by 3D-Force-Clamp Tracking of Single Kinesin-1 Motors. *Nano*

Lett. acs.nanolett.7b04971 (2018) doi:10.1021/acs.nanolett.7b04971.

43. Kim, Y. C. & Fisher, M. E. Vectorial loading of processive motor proteins: implementing a landscape picture. *J. Phys. Condens. Matter* **17**, S3821-38 (2005).

44. Kolomeisky, A. B. & Fisher, M. E. Molecular motors: a theorist's perspective. *Annu. Rev. Phys. Chem.* **58**, 675–95 (2007).

45. Fisher, M. E. & Kim, Y. C. Kinesin crouches to sprint but resists pushing. *Proc. Natl. Acad. Sci. U. S. A.* **102**, 16209–14 (2005).

46. Gittes, F., Meyhöfer, E., Baek, S. & Howard, J. Directional loading of the kinesin motor molecule as it buckles a microtubule. *Biophys. J.* **70**, 418–29 (1996).

47. Gennerich, A. & Reck-Peterson, S. L. Probing the force generation and stepping behavior of cytoplasmic dynein. *Methods Mol. Biol.* **783**, 63–80 (2011).

48. Nicholas, M. P. *et al*. Cytoplasmic dynein regulates its attachment to microtubules via nucleotide state-switched mechanosensing at multiple AAA domains. *Proc. Natl. Acad. Sci.* **112**, 6371–6376 (2015).

49. Kunwar, A., Vershinin, M., Xu, J. & Gross, S. P. Stepping, Strain Gating, and an Unexpected Force-Velocity Curve for Multiple-Motor-Based Transport. *Curr. Biol.* **18**, 1173–1183 (2008).

50. Keppler, A. *et al*. A general method for the covalent labeling of fusion proteins with small molecules in vivo. *Nat. Biotechnol.* **21**, 86–9 (2003).

51. Nitzsche, B. *et al*. *Studying kinesin motors by optical 3D-nanometry in gliding motility assays*. *Methods in Cell Biology* vol. 95 (Elsevier, 2010).

52. Ruhnow, F., Zwicker, D. & Diez, S. Tracking single particles and elongated filaments

with nanometer precision. *Biophys. J.* **100**, 2820–8 (2011).

53. Howard, J., Hudspeth, A. & Vale, R. Movement of microtubules by single kinesin molecules. *Nature* **342**, 154–158 (1989).

54. Tanner, N. a & van Oijen, A. M. Visualizing DNA replication at the single-molecule level. *Methods Enzymol.* **475**, 259–78 (2010).

55. Gell, C. *et al*. Microtubule dynamics reconstituted in vitro and imaged by single-molecule fluorescence microscopy. in *Methods in cell biology* vol. 95 221–45 (Elsevier, 2010).

56. Wong, W. P. & Halvorsen, K. The effect of integration time on fluctuation measurements: calibrating an optical trap in the presence of motion blur. *Opt. Express* **14**, 12517 (2006).